

Relaxed Total Generalized Variation Regularized Piecewise Smooth Mumford-Shah Model for Triangulated Surface Segmentation

Huayan Zhang^a, Shanqiang Wang^a, Xiaochao Wang^b

^a*School of Computer Science and Technology, Tiangong University, Tianjin, China*

^b*School of Mathematics, Tiangong University, Tianjin, China*

Abstract

The Mumford-Shah (MS) model is an important technique for mesh segmentation. Many existing researches focus on piecewise constant MS mesh segmentation model with total variation regularization, which pursue the shortest length of boundaries. Different from previous efforts, in this article, we propose a novel piecewise smooth MS mesh segmentation model by utilizing the relaxed total generalized variation regularization (rTGV). The new model assumes that the feature function of a mesh can be approximated by the sum of piecewise constant function and a smooth function, and the rTGV regularization is able to characterize the high order discontinuity of the geometric structure. The newly introduced method is effective in segmenting meshes with irregular structures and getting the better boundaries rather than the shortest boundaries. We solve the new model by alternating minimization and alternating direction method of multipliers (ADMM). Our algorithm is discussed from several aspects, and comparisons with several state-of-art methods. Experimental results show that our method can yield competitive results when compared to other approaches. In addition, our results compare favorably to those of the several state-of-art techniques when evaluated on the Princeton Segmentation Benchmark. Furthermore, the quantitative errors and computational costs confirm the robustness and efficiency of the proposed method.

Keywords: The Mumford-Shah model, Mesh segmentation, Relaxed total generalized variation, ADMM

1. Introduction

Mesh segmentation is a fundamental task in geometric modeling and computer graphics community. It has many applications such as parameterization, simplification, shape retrieval, multiresolution modeling, skeleton extraction and so on.

For a given mesh M with region Ω , mesh segmentation aims to decompose the mesh region Ω into K disjoint connected piecewise smooth subsets Ω_k with a union of smooth boundaries Γ such that

$$\Omega = \Omega_1 \cup \dots \cup \Omega_K \cup \Gamma, \quad \Omega_i \cap \Omega_j = \emptyset.$$

The pioneered Mumford-Shah (MS) segmentation model [1] finds an optimal piecewise smooth approximation u of f by the following minimization problem:

$$\min_{u, \Gamma} |\Gamma| + \beta \int_{\Omega \setminus \Gamma} |\nabla u|^2 dx + \alpha \int_{\Omega} |f - u|^2 dx, \quad (1)$$

where f is the input feature function of M , u is a piecewise smooth approximation of f , such that u varies smoothly within each Ω_i and discontinuously across the boundaries of Ω_i , and $|\Gamma|$ stands for the total boundary length.

In practice, it is very challenging to solve (1) due to its non-convex and the discontinuous of the integral regions. A classical reduced version of model (1) can be obtained by restricting u into a piecewise constant function, i.e.

$u = \sum_{k=1}^K \mu_k \gamma_k$, μ_k and γ_k are the feature value and the indicator function of region Ω_i , respectively. The reduced piecewise constant MS model can be formulated as follows

$$\min_{\{\mu_i\}, \{\Omega_i\}} \sum_i |\partial \Omega_i| + \alpha \sum_{i=1}^K \int_{\Omega} |f - \mu_i|^2 \gamma_i dx. \quad (2)$$

In addition, [2, 3] further reformulated (2) into the following optimization problem by introducing continuous multi-class label $\mathbf{u} = \{u_k\}$, with $u_k \in [0, 1]$ and $\sum_k u_k = 1$.

$$\min_{\{\mu_i, \mathbf{u}\}} \int_{\Omega} |\nabla \mathbf{u}| dx + \alpha \sum_{i=1}^K \int_{\Omega} |f - \mu_i|^2 u_i dx, \quad (3)$$

where the first term is based on the fact the perimeter of $\{\Omega_i\}$ can be expressed as the total variation of the indicator function [4].

The piecewise constant MS model (2) and (3) have been successfully applied in image segmentation [5, 6, 7, 8, 9] and mesh segmentation [10, 11]. However, for images with intensity inhomogeneity and surfaces with irregular regions, the piecewise constant MS model may get into local minima. Many variants piecewise smooth MS models are proposed to process images with intensity inhomogeneity [12, 13, 14, 15, 16, 17]. By treating the intensity inhomogeneity as small perturbation of piecewise constant intensities, the following model is proposed by decomposing the piecewise smooth function into a piecewise constant function and a smooth function.

$$f(x) = \sum_k b(x) \mu_k + n(x), x \in \Omega, \quad (4)$$

where $b(x)$ is a smooth function, and $n(x)$ is the noise.

Based on (4), [14] reformulated the MS model (1) as the following minimization problem:

$$\begin{aligned} \min_{\{b, \Omega_k, \mu_k\}} \sum_k (|\partial \Omega_k| + \frac{\alpha}{2} \int_{\Omega_k} (f - b \mu_k)^2 + \omega(f - \mu_k)^2 dx) \\ + \beta \int_{\Omega} |\nabla b|^2 dx. \end{aligned} \quad (5)$$

In addition, the smooth function in (4) can be defined as the following additive way [12, 15, 16, 17]

$$f(x) = \sum_k \mu_k \gamma_k(x) + b(x) + n(x). \quad (6)$$

Relying on (6), [12] proposed the following problem:

$$\begin{aligned} \min_{\{b, \Omega_k, \mu_k\}} \sum_k (|\partial \Omega_k| + \frac{\alpha}{2} \int_{\Omega_k} (f - \mu_k - b)^2 dx) + \frac{\beta}{2} \int_{\Omega} |\nabla b|^2 dx \\ + \frac{\eta}{2} \int_{\Omega} |\nabla^2 b|^2 dx. \end{aligned} \quad (7)$$

[16] proposed a piecewise smooth MS model with the L_1 fidelity term instead of the L_2 term. [17] built up the following piecewise smooth MS model by utilizing a non-convex L^p ($0 \leq p \leq 1$) regularity term and a laplace smooth term.

$$\begin{aligned} \min_{\{b, \mathbf{u}, \mu\}} \int_{\Omega} |\nabla \mathbf{u}|^p dx + \frac{\beta}{2} \int_{\Omega} |\Delta b|^2 dx + \frac{\eta}{2} \int_{\Omega} |b|^2 dx \\ + \alpha \sum_k \int_{\Omega_k} \langle (f - b - \mu_k)^2, \mathbf{u} \rangle dx. \end{aligned} \quad (8)$$

The above piecewise smooth MS models have been demonstrated to be effective in dealing with images with intensity inhomogeneity, which try to obtain the shortest length of boundaries $|\Gamma|$ with the total variation regularization (TV). However, as the surface is irregular, the shortest boundaries sometimes are not necessarily the optimal segmentation boundaries. Recently, the second order relaxed total generalized variation (TGV/rTGV) regularization [18, 19] on images and meshes has been proven to be able to capture the first-order discontinuity structures of a function and alleviate the stair-case effects of TV regularization effectively (See Figure 1 for an example. For the one-dimensional

noisy signal, the TV method cannot restore the vertex at the first-order discontinuity, but TGV can preserve the vertex well)

Motivated by the good properties of the TGV/rTGV regularization, in the paper, we consider the rTGV regularized piecewise smooth MS mesh segmentation method to pursue better boundaries rather than just the shortest boundaries. To the best of our knowledge, there is little research on rTGV regularized piecewise smooth MS model technique for triangulated surface segmentation ([20] proposes to use the piecewise linear TGV regularization for segmenting point cloud data. However, due to the lack of inherent topological structure in point clouds, the piecewise linear TGV regularization defined on them cannot guarantee convergence. As a result, the segmentation outcomes on point cloud data are often unsatisfactory). The variational model is a new discretization of the classical piecewise smooth Mumford-Shah model by applying rTGV regularization on triangle meshes. Besides, we use a simple alternating minimization and ADMM to solve the non-convex problem. Plenty of experiments showed this new segmentation method works well, which always gives satisfying segmentation results with correct human perception.

2. Related work

2.1. Mesh segmentation

Mesh segmentation is an important basic topic in geometric modeling and computer graphics community. With different applications, mesh segmentations can be divided into surface-type and part-type segmentations. For surface-type segmentation, a mesh surface is partitioned into basic mathematical structures such as planes and spheres. For part-type segmentation, a mesh surface is partitioned into meaningful volumetric parts which respect human perception. So far a wide variety of algorithms have been developed for decomposing meshes. The interested reader can refer to excellent surveys [21, 22, 23, 24], and a benchmark for evaluating mesh segmentation algorithms [25], as well as some recent developments, which mainly include traditional variational-based method [26, 10, 27, 28, 29, 30] and learning-based segmentation [31, 32, 33, 34, 35].

Isoline Cut [26] proposes to get the isolines of the concave-aware segmentation field with higher scores as the final contour. The method is effective. However, it is not suitable for segmenting CAD meshes. [10] discretizes the piecewise constant Mumford-Shah image segmentation [1] to get a vertex-based mesh segmentation method. As the Mumford-Shah model is a famous non-convex model, the solution severely depends on the initialization. The segmentation method in [27] proposed a greedy algorithm by first over segmenting the models into approximate convex components, and then merging process and refining to achieve final segmentation. [28] proposed the Mumford-Shah mesh processing method by using the ambrosio tortorelli functional. The authors of [29] proposed a new spectral mesh segmentation method via L_0 minimization. The method adopt a coarse-to-fine strategy, first devising a heuristic algorithm to find a coarse segmentation, then proposing an optimization algorithm to refine the segment boundaries. The algorithm can produce satisfying results, but it involves many parameters. [30] introduced a new total variation diffusion method to get the segmentation results, which is quite simple. However, the method is affected by initializations. While obtaining good results, most variational-based segmentation methods involve multiple step operations with higher computational cost. Some are still either unstable, or sensitive to initializations, or even need user interaction.

Recently, the deeping learning techniques have been studied for mesh segmentation. The pioneered learning-based segmentation method [31] proposed to get segmentation results using labeling techniques, which can get excellent results. The authors further improved the method by using the convolutional networks [32]. The method in [33] proposed the coherent segmentation method based on the convolutional neural networks and a two-layer long short term memory. In addition, [34] proposed a novel representation of meshes by random walks along the surface, and then devised an end-to-end learning framework that realizes the representation within Recurrent Neural Network. Furthermore, by mapping the input mesh surface to the multi-dimensional Laplacian-Beltrami space, [35] introduce the Laplacian2Mesh framework for shape classification and segmentation. Overall, the learning-based methods can effectively process different types of data, and get better classification results. However, the learning-based methods rely on large number of datasets, and the computational costs are higher.

In the paper, we focus on the rTGV regularized piecewise smooth MS mesh segmentation method, which belongs to the traditional variational-based method. The method combines the piecewise smooth MS model and rTGV regularization.

2.2. Our contributions and paper organization

The existing researches on piecewise constant MS mesh segmentation method with TV regularization seek the shortest length of boundaries. Different from previous work, the goal of this paper is to investigate the piecewise smooth Mumford-Shah mesh segmentation model with the total generalized variation regularization, in order to obtain the better boundaries instead of the shortest boundaries.

- We propose the rTGV regularized piecewise smooth MS model for triangulated surface segmentation method (containing the first order TV and the second order RTGV).
- The optimization problem is solved by the alternating minimization and alternating direction method of multipliers.
- Our algorithm is discussed and compared to several state-of-art methods in various aspects. Experimental results show that our piecewise smooth MS method can yield competitive results when compared to piecewise constant MS method, and other approaches on the Princeton Segmentation Benchmark. Furthermore, the quantitative errors and computational costs confirm the robustness and efficiency of the proposed method.

The remainder of the paper is organized as follows. Section 2 gives some notations, differential operators on mesh and the definition of TV/rTGV regularization. In section 3, we introduce our TGV regularized piecewise smooth MS mesh segmentation method. Section 4 presents the details for solving our segmentation optimization problem. In section 5, we present the experiments and comparisons. Section 6 concludes the paper.

3. The Relaxed Total Generalized Variation Regularization

In the section, we introduce some notations followed by differential operators and the general total variation regularization on triangulated surfaces.

3.1. Notations

Without loss of generality, we denote a triangulated surface with no degenerate triangles as $M \subset \mathbb{R}^3$. The set of vertices, edges and triangles of M are denoted as $\{v_i : i = 0, 1, \dots, V_M - 1\}$, and $\{e_i : i = 0, 1, \dots, E_M - 1\}$, and $\{\tau_i : i = 0, 1, \dots, T_M - 1\}$. Here V_M , E_M and T_M are the numbers of vertices, edges and triangles, respectively. If v is an endpoint of an edge e , then we denote it as $v < e$. Similarly, if e is an edge of a triangle τ , it is denoted as $e < \tau$. For each edge e , we choose a direction arbitrarily. If the direction of e is consistent with its connecting triangle τ , we denote $\text{sgn}(\tau, e) = 1$, else $\text{sgn}(\tau, e) = -1$. Denote $N_2(\tau)$ as the second type 1-neighborhood of triangle τ , which are the triangles sharing some common vertex with τ .

3.2. Differential operators on mesh

We first present the definitions of gradient operator and divergence operator on the triangulated surface. Two types of regularization are then given based on these operators (see [36], and [19] for details).

We first denote the space $\mathbf{U}_M = \mathbf{R}^{T_M \times n}$. For $\mathbf{u} = (\mathbf{u}_0, \dots, \mathbf{u}_\tau, \dots, \mathbf{u}_{T_M-1}) \in \mathbf{U}_M$, $\mathbf{u}_\tau = (u_{\tau,1}, \dots, u_{\tau,n})$ is a n -dimensional vector. For each edge e , the gradient operators ∇ restricted on each edge e has the following form:

$$(\nabla \mathbf{u})_e = \begin{cases} \sum_{\tau < e} \mathbf{u}_\tau \text{sgn}(\tau, e), & e \not\subseteq \partial M, \\ 0, & e \subseteq \partial M. \end{cases} \quad (9)$$

We then denote the range of ∇ as \mathbf{V}_M . For $\mathbf{p} \in \mathbf{V}_M$, as the adjoint operator of ∇ is $-\text{div}$, we then have the following divergence operator for M .

$$(\text{div}(\mathbf{p}))_\tau = \frac{-1}{A_\tau} \sum_{e < \tau} \mathbf{p}_e \text{sgn}(\tau, e) l_e, \quad (10)$$

where A_τ is the area of triangle τ , and l_e is the length of edge e .

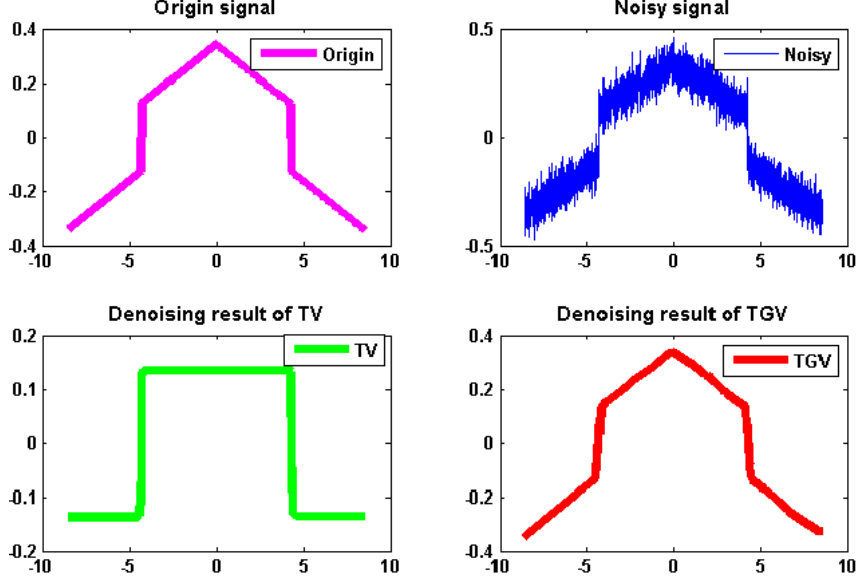


Figure 1: The comparison between TV regularization and TGV regularization.

3.3. Relaxed Total generalized variation regularization

According to the above operators (9) and (10), we present the following total generalized variation regularization (TGV^p , $p = 1, 2$ indicating the order information), which contains the first order total variation regularization ($\text{TGV}^1 = \text{TV}$) and the second order relaxed total generalized variation regularization ($\text{TGV}^2 = \text{RTGV}$).

For $\mathbf{u} \in \mathbf{U}_M$, $\mathbf{v} \in \mathbf{V}_M$, we then have

$$\begin{aligned}
 \text{TGV}^1(\mathbf{u}) &= \text{TV}(\mathbf{u}) = \|\nabla \mathbf{u}\|_1 = \sum_e \sum_{i=1}^n |(\nabla \mathbf{u})_{ei}| l_e, \\
 \text{TGV}^2(\mathbf{u}) &= \text{RTGV}(\mathbf{u}) = \min_{\mathbf{v}} \|\nabla \mathbf{u} - \mathbf{v}\|_1 + \alpha_0 \|\text{div}(\mathbf{v})\|_1 \\
 &= \min_{\mathbf{v}} \sum_e \sum_{i=1}^n |(\nabla \mathbf{u} - \mathbf{v})_{ei}| l_e + \alpha_0 \sum_{\tau} \sum_{i=1}^n |\text{div}(\mathbf{v})_{\tau i}| A_{\tau}.
 \end{aligned} \tag{11}$$

The TV regularization has been applied for mesh denoising [36] and piecewise constant MS mesh segmentation [10, 11]. However, for meshes with ambiguous semantic information or irregular regions (for the meshes in Fig. 5,6), the piecewise constant MS mesh segmentation methods may fall into local minima, and have difficulty in getting the better segmentation boundaries. The RTGV regularization has been applied for mesh denoising [19], and is able to recover the first order discontinuity of a signal and overcome the stair-case artifacts (false edges) of TV regularization. In the following, we focus on TGV^p regularized piecewise smooth MS mesh segmentation method to obtain better segmentation boundaries other than the shortest boundaries.

4. TGV^p regularized piecewise smooth MS mesh segmentation method

As mentioned before, for a mesh M with region Ω to be divided into \mathbf{K} disjoint parts $\{\Omega_k\}_{k=1}^{\mathbf{K}}$, the piecewise smooth MS model tries to approximate feature function of M by $\mathbf{g}(x) = \sum_k \mu_k \mathbf{u} + \mathbf{b}$: piecewise constant values $\{\mu_k\}$ and a smooth function \mathbf{b} .

4.1. The feature function \mathbf{f} of mesh

A popular way to define the feature functions of images and meshes is using the spectral space, which is spanned by the eigenvectors of a Laplacian matrix [37, 38, 39, 10, 11]. In the paper, we adopt the high order Laplacian matrix in [11] to construct the feature function \mathbf{f} , which involved two-type neighborhood normals N_2 .

Specifically, for a given mesh, the Laplacian matrix $L = [L_{ij}]$ in [11] is given as follows:

$$L_{ij} = \begin{cases} -w_{ij}, & i \neq j \text{ and } \tau_i, \tau_j \text{ share an edge,} \\ \sum_k w_{i,k}, & i = j \text{ and } k \in N_1(\tau_i), \\ 0, & \text{otherwise,} \end{cases} \quad (12)$$

where $w_{ij} = l_e \exp(-\frac{d(\tau_i, \tau_j)}{\bar{d}})$, \bar{d} being the average of $d(\tau_i, \tau_j)$ over all edges, and $d(\tau_i, \tau_j)$ denotes the error between normals. In Fig. 5,6, we present the feature functions of the two meshes.

4.2. Piecewise smooth MS mesh segmentation method

By introducing a multi-continuous label $\mathbf{u} \in C_{\mathbf{u}} = \{\mathbf{u}_{\tau} | u_{\tau,k} \geq 0, \sum_{k=1}^{\mathbf{K}} u_{\tau,k} = 1, \forall \tau\} \subset \mathbf{U}_M$, we then obtain the following piecewise smooth MS mesh segmentation optimization problem.

$$\begin{aligned} \min_{\mathbf{u} \in C_{\mathbf{u}}, \mathbf{b}, \mu} E(\mathbf{u}, \mathbf{b}, \mu) \\ = \text{TGV}^p(\mathbf{u}) + \frac{\beta}{2} \|\Delta \mathbf{b}\|_{\mathbf{U}_M}^2 + \frac{\eta}{2} \|\mathbf{b}\|_{\mathbf{U}_M}^2 + \frac{\alpha}{2} \langle \mathbf{u}, s(\mathbf{f}, \mathbf{b}, \mu) \rangle_{\mathbf{U}_M}, \end{aligned} \quad (13)$$

where the second term is to get the smooth parts of \mathbf{f} , the third term is used to stabilize the \mathbf{b} sub problem, the last term is the similarity term, and $s(\mathbf{f}, \mathbf{b}, \mu) = \{s_{\tau}(\mathbf{f}, \mathbf{b}, \mu)\}$ with $s_{\tau}(\mathbf{f}, \mathbf{b}, \mu) = \{\|\mathbf{f}_{\tau} - \mathbf{b}_{\tau} - \mu_k\|^2\}_{k=1}^{\mathbf{K}}$, \mathbf{f} is the eigenvectors of the smallest $\mathbf{K} - 1$ eigenvalues of the Laplace matrix, and β, η, α are positive parameters. As (13) is non-convex, the solution is not unique. Motivated by the techniques of [16, 17], it is still available to show the existence of minimizers of (13).

Theorem 1. *Let Ω be a bounded subset of R^3 with a Lipschitz boundary. Assume that \mathbf{f} and $\{\mu_k\}_{k=1}^{\mathbf{K}}$ are bounded. Then, for $\beta, \eta, \alpha > 0$, there exists a minimizer $(\mathbf{u}^*, \mathbf{b}^*, \mu^*)$ for problem (13). (The proof is shown in the APPENDIX)*

4.3. Alternating minimization method (AMM) for solving (13)

Given the following function

$$\chi(\mathbf{u}) = \begin{cases} 0, & \mathbf{u} \in C_{\mathbf{u}} \\ +\infty, & \mathbf{u} \notin C_{\mathbf{u}}, \end{cases} \quad (14)$$

the minimization problem (13) can be solved alternately by the following two optimization problems.

- For fixed μ : \mathbf{u}, \mathbf{b} can be obtained by solving

$$\min_{\mathbf{u}, \mathbf{b}, \mu} \text{TGV}^p(\mathbf{u}) + \frac{\beta}{2} \|\Delta \mathbf{b}\|_{\mathbf{U}_M}^2 + \frac{\eta}{2} \|\mathbf{b}\|_{\mathbf{U}_M}^2 + \frac{\alpha}{2} \langle \mathbf{u}, s(\mathbf{f}, \mathbf{b}, \mu) \rangle_{\mathbf{U}_M} + \chi(\mathbf{u}), \quad (15)$$

which is non-differentiable, and can be efficiently solved by augmented Lagrangian method (ALM) or alternating direction multiplier method (ADMM) [40, 41, 42, 43]; see section 5 for details.

- For fixed \mathbf{u}, \mathbf{b} : μ can be obtained by solving

$$\min_{\mu} \frac{\alpha}{2} \langle \mathbf{u}, s(\mathbf{f}, \mathbf{b}, \mu) \rangle_{\mathbf{U}_M},$$

and is exactly

$$\mu_k = \frac{\sum_{\tau} u_{k,\tau} (\mathbf{f}_{\tau} - \mathbf{b}_{\tau}) A_{\tau}}{\sum_{\tau} u_{k,\tau} A_{\tau}}, \quad k = 0, 1, \dots, \mathbf{K}. \quad (16)$$

In our implementation, the alternating minimization method is listed in Algorithm 1.

Algorithm 1 AMM for solving (13)

htbp

1. Initialization:

- μ^{-1} : computed according to the technique in [11];
- \mathbf{u}^{-1} : obtained by μ^0 ;
- $\mathbf{v}^{-1} = 0$, $\mathbf{b}^{-1} = 0$, $\mathbf{p}^{-1} = 0$, $\mathbf{q}^{-1} = 0$, $\mathbf{z}^{-1} = 0$,
 $\lambda_{\mathbf{p}}^{-1} = 0$, $\lambda_{\mathbf{q}}^{-1} = 0$, $\lambda_{\mathbf{z}}^{-1} = 0$, $l = -1$;

2. Repeat

- For fixed μ^{l-1} , computing
($\mathbf{u}^l, \mathbf{v}^l, \mathbf{b}^l, \mathbf{p}^l, \mathbf{q}^l, \mathbf{z}^l, \lambda_{\mathbf{p}}^l, \lambda_{\mathbf{q}}^l, \lambda_{\mathbf{z}}^l$) by solving (15) through Algorithm 2;
- For fixed ($\mathbf{u}^l, \mathbf{b}^l$), computing μ^l from (16);

Until ($\|\mathbf{u}^{n+1} - \mathbf{u}^n\|_{\mathbf{U}_M}^2 < 10^{-5}$).

3. Classify \mathbf{u} by the method in [3].

5. Algorithm details for solving (15)

Generally, in the following, we only present the details for solving (15) with $p = 2$ (RTGV regularization). By introducing three auxiliary variables $\mathbf{p} \in \mathbf{V}_M$ and $\mathbf{q}, \mathbf{z} \in \mathbf{U}_M$. The problem (15) with $p = 2$ can be further written as

$$\begin{aligned} \min_{\substack{\mathbf{u}, \mathbf{b} \in \mathbf{U}_M, \mathbf{v} \in \mathbf{V}_M, \\ \mathbf{p} \in \mathbf{V}_M, \mathbf{q}, \mathbf{z} \in \mathbf{U}_M}} \quad & \|\mathbf{p}\|_1 + \alpha_0 \|\mathbf{q}\|_1 + \frac{\beta}{2} \|\Delta \mathbf{b}\|_{\mathbf{U}_M}^2 + \frac{\eta}{2} \|\mathbf{b}\|_{\mathbf{U}_M}^2 + \frac{\alpha}{2} (\mathbf{z}, \mathbf{s}(\mathbf{f}, \mathbf{b}, \mu))_{\mathbf{U}_M} + \chi(\mathbf{z}), \\ \text{s.t.} \quad & \mathbf{p} = \nabla \mathbf{u} - \mathbf{v}, \quad \mathbf{q} = \text{div}(\mathbf{v}), \quad \mathbf{z} = \mathbf{u}. \end{aligned} \quad (17)$$

To solve (17) effectively, we define the following augmented Lagrangian functional:

$$\begin{aligned} \mathcal{L}(\mathbf{u}, \mathbf{v}, \mathbf{b}, \mathbf{p}, \mathbf{q}, \mathbf{z}; \lambda_{\mathbf{p}}, \lambda_{\mathbf{q}}, \lambda_{\mathbf{z}}) = & \|\mathbf{p}\|_1 + \alpha_0 \|\mathbf{q}\|_1 + \frac{\beta}{2} \|\Delta \mathbf{b}\|_{\mathbf{U}_M}^2 + \frac{\eta}{2} \|\mathbf{b}\|_{\mathbf{U}_M}^2 \\ & + \frac{\alpha}{2} (\mathbf{z}, \mathbf{s}(\mathbf{f}, \mathbf{b}, \mu))_{\mathbf{U}_M} + \chi(\mathbf{z}) + (\lambda_{\mathbf{p}}, \mathbf{p} - (\nabla \mathbf{u} - \mathbf{v}))_{\mathbf{V}_M} \\ & + \frac{r_{\mathbf{p}}}{2} \|\mathbf{p} - (\nabla \mathbf{u} - \mathbf{v})\|_{\mathbf{V}_M}^2 + (\lambda_{\mathbf{q}}, \mathbf{q} - \text{div}(\mathbf{v}))_{\mathbf{U}_M} + \frac{r_{\mathbf{q}}}{2} \|\mathbf{q} - \text{div}(\mathbf{v})\|_{\mathbf{U}_M}^2 \\ & + (\lambda_{\mathbf{z}}, \mathbf{z} - \mathbf{u})_{\mathbf{U}_M} + \frac{r_{\mathbf{z}}}{2} \|\mathbf{z} - \mathbf{u}\|_{\mathbf{U}_M}^2, \end{aligned} \quad (18)$$

where $r_{\mathbf{p}}, r_{\mathbf{q}}$ and $r_{\mathbf{z}}$ are positive parameters.

The solution of (18) is equivalent to the following saddle-point problem

$$\max_{\lambda_{\mathbf{p}}, \lambda_{\mathbf{q}}, \lambda_{\mathbf{z}}} \min_{\substack{\mathbf{u}, \mathbf{v}, \mathbf{b}, \\ \mathbf{p}, \mathbf{q}, \mathbf{z}}} \mathcal{L}(\mathbf{u}, \mathbf{v}, \mathbf{b}, \mathbf{p}, \mathbf{q}, \mathbf{z}; \lambda_{\mathbf{p}}, \lambda_{\mathbf{q}}, \lambda_{\mathbf{z}}), \quad (19)$$

which can be iteratively solved by splitting (19) into the following several subproblems.

5.1. Sub-minimizations with respect to $\mathbf{u}, \mathbf{v}, \mathbf{b}$

The $\mathbf{u}, \mathbf{v}, \mathbf{b}$ sub-problems are reformulated as follows

$$\min_{\mathbf{u} \in \mathbf{U}_M} (\lambda_{\mathbf{p}}, -\nabla \mathbf{u})_{\mathbf{V}_M} + (\lambda_{\mathbf{z}}, -\mathbf{u})_{\mathbf{U}_M} + \frac{r_{\mathbf{p}}}{2} \|\mathbf{p} - (\nabla \mathbf{u} - \mathbf{v})\|_{\mathbf{V}_M}^2 + \frac{r_{\mathbf{z}}}{2} \|\mathbf{z} - \mathbf{u}\|_{\mathbf{U}_M}^2, \quad (20)$$

$$\min_{\mathbf{v} \in \mathbf{Q}_M} (\lambda_{\mathbf{q}}, -\text{div}(\mathbf{v}))_{\mathbf{U}_M} + \frac{r_{\mathbf{q}}}{2} \|\mathbf{q} - \text{div}(\mathbf{v})\|_{\mathbf{U}_M}^2 + (\lambda_{\mathbf{p}}, \mathbf{v})_{\mathbf{V}_M} + \frac{r_{\mathbf{p}}}{2} \|\mathbf{p} - (\nabla \mathbf{u} - \mathbf{v})\|_{\mathbf{V}_M}^2, \quad (21)$$

$$\min_{\mathbf{b} \in \mathbf{U}_M} \frac{\alpha}{2} (\mathbf{z}, \mathbf{s}(\mathbf{f}, \mathbf{b}, \mu))_{\mathbf{U}_M} + \frac{\beta}{2} \|\Delta \mathbf{b}\|_{\mathbf{U}_M}^2 + \frac{\eta}{2} \|\mathbf{b}\|_{\mathbf{U}_M}^2. \quad (22)$$

The above sub-problems are quadratic programming problems, and can be solved by various numerical packages, such as MKL, Taucs and Eigen.

5.2. Sub-minimizations with respect to $\mathbf{p}, \mathbf{q}, \mathbf{z}$

Specifically, the $\mathbf{p}, \mathbf{q}, \mathbf{z}$ sub-problems can be reformulated as follows and solved with the closed form solutions.

- For \mathbf{p} sub-problem, we have

$$\min_{\mathbf{p} \in \mathbf{V}_M} \|\mathbf{p}\|_1 + (\lambda_{\mathbf{p}}, \mathbf{p})_{\mathbf{V}_M} + \frac{r_{\mathbf{p}}}{2} \|\mathbf{p} - (\nabla \mathbf{u} - \mathbf{v})\|_{\mathbf{V}_M}^2. \quad (23)$$

It has the following closed form solution

$$\forall e, \mathbf{p}_e = \begin{cases} (1 - \frac{1}{r_{\mathbf{p}}|\mathbf{w}_e|})\mathbf{w}_e, & |\mathbf{w}_e| > \frac{1}{r_{\mathbf{p}}}, \\ 0, & |\mathbf{w}_e| \leq \frac{1}{r_{\mathbf{p}}}, \end{cases} \quad (24)$$

where $\mathbf{w}_e = (\nabla \mathbf{u} - \mathbf{v} - \frac{\lambda_{\mathbf{p}}}{r_{\mathbf{p}}})|_e$.

- For \mathbf{q} sub-problem, we have

$$\min_{\mathbf{q} \in \mathbf{U}_M} \alpha_0 \|\mathbf{q}\|_1 + (\lambda_{\mathbf{q}}, \mathbf{q})_{\mathbf{U}_M} + \frac{r_{\mathbf{q}}}{2} \|\mathbf{q} - \text{div}(\mathbf{v})\|_{\mathbf{U}_M}^2, \quad (25)$$

which has the following closed form solution

$$\forall \tau, \mathbf{q}_{\tau} = \begin{cases} (1 - \frac{\alpha_0}{r_{\mathbf{q}}|\mathbf{c}_{\tau}|})\mathbf{c}_{\tau}, & |\mathbf{c}_{\tau}| > \frac{\alpha_0}{r_{\mathbf{q}}}, \\ 0, & |\mathbf{c}_{\tau}| \leq \frac{\alpha_0}{r_{\mathbf{q}}}, \end{cases} \quad (26)$$

where $\mathbf{c}_{\tau} = \text{div}(\mathbf{v}) - \frac{\lambda_{\mathbf{q}}}{r_{\mathbf{q}}}$.

- For \mathbf{z} sub-problem, we get

$$\min_{\mathbf{z} \in \mathbf{U}_M} \alpha (\mathbf{z}, \mathbf{s}(\mathbf{f}, \mu, \mathbf{b}))_{\mathbf{U}_M} + \chi(\mathbf{z}) + (\lambda_{\mathbf{z}}, \mathbf{z})_{\mathbf{U}_M} + \frac{r_{\mathbf{z}}}{2} \|\mathbf{z} - \mathbf{u}\|_{\mathbf{U}_M}^2. \quad (27)$$

It can be solved through

$$\mathbf{z} = \text{Proj}_{\mathbf{C}_u}(\mathbf{u} - \frac{\alpha \mathbf{s}(\mathbf{f}, \mathbf{b}, \mu) + \lambda_{\mathbf{z}}}{r_{\mathbf{z}}}), \quad (28)$$

which can be calculated via Michelot's algorithm [44].

The whole algorithm for solving (19) is listed in Algorithm 2. As the MS segmentation optimization problem (17) is non-convex, it is difficult to show the convergence of our algorithm. Similar to the theorems given in [16, 17], we can only get the following partial convergence theorem.

Theorem 2. *Supposed $\mathbf{u}^l - \mathbf{u}^{l-1} \rightarrow 0, \mathbf{v}^l - \mathbf{v}^{l-1} \rightarrow 0, \lambda_{\mathbf{p}}^l - \lambda_{\mathbf{p}}^{l-1} \rightarrow 0, \lambda_{\mathbf{q}}^l - \lambda_{\mathbf{q}}^{l-1} \rightarrow 0, \lambda_{\mathbf{z}}^l - \lambda_{\mathbf{z}}^{l-1} \rightarrow 0$, in Algorithm 1. If the sequence $\{(\mathbf{u}^l, \mathbf{v}^l, \mathbf{b}^l, \mu^l, \mathbf{p}^l, \mathbf{q}^l, \mathbf{z}^l, \lambda_{\mathbf{p}}^l, \lambda_{\mathbf{q}}^l, \lambda_{\mathbf{z}}^l)\}$ generated by the Algorithm 1 converges to a limit point $(\mathbf{u}^*, \mathbf{v}^*, \mathbf{b}^*, \mu^*, \mathbf{p}^*, \mathbf{q}^*, \mathbf{z}^*, \lambda_{\mathbf{p}}^*, \lambda_{\mathbf{q}}^*, \lambda_{\mathbf{z}}^*)$, then the limit point satisfies the following Karush-Kuhn-Tucker (KKT) conditions of (17):*

$$\left\{ \begin{array}{l} -\lambda_{\mathbf{z}}^* + \text{div}(\lambda_{\mathbf{p}}^*) = 0, \\ \lambda_{\mathbf{p}}^* + \nabla(\lambda_{\mathbf{q}}^*) = 0, \\ (\beta \Delta^2 + \eta \mathcal{I} + \alpha \mathcal{I})\mathbf{b}^* + \alpha < -(\mathbf{f} - \mu^*), \mathbf{z}^* > = 0, \\ \alpha < \mu^* - (\mathbf{f} - \mathbf{b}^*), \mathbf{u}^* > = 0, \\ \partial(\|\mathbf{p}^*\|_1) + \lambda_{\mathbf{p}}^* = 0, \\ \alpha_0 \partial(\|\mathbf{q}^*\|_1) + \lambda_{\mathbf{q}}^* = 0, \\ \alpha s(\mathbf{f}, \mathbf{b}^*, \mu^*) + \lambda_{\mathbf{z}}^* + \partial\chi(\mathbf{z}^*) = 0, \\ \mathbf{p}^* - (\nabla \mathbf{u}^* - \mathbf{v}^*) = 0, \\ \mathbf{q}^* - \text{div}(\mathbf{v}^*) = 0, \\ \mathbf{z}^* - \mathbf{u}^* = 0, \end{array} \right. \quad (29)$$

Algorithm 2 ADMM for solving (19)

1. Initialization:

- $\mathbf{u}^{l,0} = \mathbf{u}^{l-1}, \mathbf{v}^{l,0} = \mathbf{v}^{l-1}, \mathbf{b}^{l,0} = \mathbf{b}^{l-1}, \mathbf{p}^{l,0} = \mathbf{p}^{l-1}, \mathbf{q}^{l,0} = \mathbf{q}^{l-1}, \mathbf{z}^{l,0} = \mathbf{z}^{l-1};$
- $\lambda_{\mathbf{p}}^{l,0} = \lambda_{\mathbf{p}}^l, \lambda_{\mathbf{q}}^{l,0} = \lambda_{\mathbf{q}}^l, \lambda_{\mathbf{z}}^{l,0} = \lambda_{\mathbf{z}}^l, K = 5;$

2. For $k = 1, 2, \dots, K$

- **z-subproblem:** For fixed $(\lambda_{\mathbf{z}}^{l,k}, \mathbf{u}^{l,k}, \mathbf{b}^{l,k})$, compute $\mathbf{z}^{l,k+1}$ from (28);
- **u-subproblem:** For fixed $(\lambda_{\mathbf{p}}^{l,k}, \lambda_{\mathbf{z}}^{l,k}, \mathbf{p}^{l,k}, \mathbf{v}^{l,k}, \mathbf{z}^{l,k+1})$, compute $\mathbf{u}^{l,k+1}$ by solving (20);
- **v-subproblem:** For fixed $(\lambda_{\mathbf{p}}^{l,k}, \lambda_{\mathbf{q}}^{l,k}, \mathbf{p}^{l,k}, \mathbf{q}^{l,k}, \mathbf{u}^{l,k+1})$, compute $\mathbf{v}^{l,k+1}$ by solving (21);
- **b-subproblem:** For fixed $(\mathbf{z}^{l,k+1})$, compute $\mathbf{b}^{l,k+1}$ by solving (22);
- **p-subproblem:** For fixed $(\lambda_{\mathbf{p}}^{l+1,k}, \mathbf{v}^{l,k+1}, \mathbf{u}^{l,k+1})$, compute $\mathbf{p}^{l,k+1}$ from (24);
- **q-subproblem:** For fixed $(\lambda_{\mathbf{q}}^{l+1,k}, \mathbf{v}^{l,k+1})$, compute $\mathbf{q}^{l,k+1}$ from (26);
- **Update Lagrange multipliers;**
 $\lambda_{\mathbf{p}}^{l,k+1} = \lambda_{\mathbf{p}}^{l,k} + r_{\mathbf{p}}(\mathbf{p}^{l,k+1} + \mathbf{v}^{l,k+1} - \nabla \mathbf{u}^{l,k+1});$
 $\lambda_{\mathbf{q}}^{l,k+1} = \lambda_{\mathbf{q}}^{l,k} + r_{\mathbf{q}}(\mathbf{q}^{l,k+1} - \text{div}(\mathbf{v}^{l,k+1}));$
 $\lambda_{\mathbf{z}}^{l,k+1} = \lambda_{\mathbf{z}}^{l,k} + r_{\mathbf{z}}(\mathbf{u}^{l,k+1} - \mathbf{z}^{l,k+1});$

3. $\mathbf{u}^l = \mathbf{u}^{l,K}, \mathbf{v}^l = \mathbf{v}^{l,K}, \mathbf{b}^l = \mathbf{b}^{l,K}, \mathbf{p}^l = \mathbf{p}^{l,K}, \mathbf{q}^l = \mathbf{q}^{l,K}, \mathbf{z}^l = \mathbf{z}^{l,K},$

$$\lambda_{\mathbf{p}}^l = \lambda_{\mathbf{p}}^{l,K}, \lambda_{\mathbf{q}}^l = \lambda_{\mathbf{q}}^{l,K}, \lambda_{\mathbf{z}}^l = \lambda_{\mathbf{z}}^{l,K}.$$

(The proof is shown in the APPENDIX)

6. Experimental results and discussions

In this section, we present experiments of our piecewise smooth MS segmentation method on a wide variety of mesh surfaces, including of the Princeton Segmentation Benchmark [25] and some other surfaces (meshes in Fig. 11). Our segmentation methods are denoted as “PSMS” (piecewise smooth MS method based on the TV regularization) and “GPSMS” (piecewise smooth MS method based on the RTGV regularization), respectively. The experiments of our algorithms and the method in [11] are conducted using Microsoft Visual Studio 2010 on a desktop with Intel(R) Core(TM) i7-8850 CPU @2.60GHz and 16GB memory and all mesh surfaces were rendered using flat shading.

We discuss our algorithm from several aspects, such as choices of parameters and comparisons to existing techniques by visual effects and quantitative errors. Specifically, we compare our segmentation method with Isoline Cut [26], WCseg [27], PCMS (piecewise constant MS) [11], Spectral L_0 [29], and two learning based methods SB19 [31]. All the segmentation results are provided by the authors. In addition, for evaluating segmentation results, we use the four evaluation metrics in [25].

6.1. Parameters and the number of segments

There are seven parameters in our algorithm: $\alpha, \beta, \alpha_0, \eta, r_{\mathbf{p}}, r_{\mathbf{q}}$ and $r_{\mathbf{z}}$. Therein $\alpha_0, \alpha, \beta, \eta$ are variational model parameters; $r_{\mathbf{p}}, r_{\mathbf{q}}, r_{\mathbf{z}}$ are optimization algorithmic parameters. The parameters $\eta, r_{\mathbf{p}}, r_{\mathbf{q}}$ and $r_{\mathbf{z}}$ can be fixed by $\eta = 0.00001, r_{\mathbf{p}} = 1, r_{\mathbf{q}} = 1, r_{\mathbf{z}} = 100$. Moreover, α, β and α_0 all have an impact on the segmentation results. According to lots of experimental tests, the parameter settings of α, β and α_0 are summarized as follows.

Firstly, the parameter α affects the segmentation boundary. Fig. 2 presents the impact of the parameter α on the results. As shown, the larger the α is, the better the segmentation boundary is. However, when the α is too large, the algorithm may over segment the mesh (see the result with $\alpha = 5 \times 10^7$ in Fig. 2). In addition, according to our tests,

the number of segment \mathbf{K} , the similarity term and the regularization term in (13) all affect the selection of α . based on these facts, we then provide the following empirical formula to estimate the α .

$$\alpha = 2 \times \mathbf{K} \times \frac{(\text{TGV})(\mathbf{u}^{-1})}{(\mathbf{u}^{-1}, \mathbf{s}(\mathbf{f}, \mathbf{b}^{-1}, \mu^{-1}))_{\mathbf{U}_M}}. \quad (30)$$

Experiments demonstrate that the empirical formula works well for many situations. In Fig. 2, we present the result produced with α computed by (30) (see the results marked by the red frame). As seen, the segmentation result with $\alpha = 4.017 \times 10^6$ is quite satisfying and the segmentation boundaries are consistent with human perception.

Secondly, the parameter β plays an important impact on the results. Experiment indicates that β is associated with α . According to the tests, there exist a range of β for our algorithm giving good segmentation results. Specifically, if the initial segmentation boundary is redundant (see the first row in Fig. 3), β should be larger than α . If the initial segmentation boundary is far from the optimal boundary (see the second row in Fig. 3), β should be smaller than α . We then have $\beta \in [0.2\alpha, 10\alpha]$. Fig. 3 presents the results of different β with other parameters fixed, which is consistent with the estimated interval.

Finally, α_0 also affect on the segmentation result, especially for meshes with poor quality. Fig. 4 show the results of different α_0 with other parameters. As seen, whether α_0 is too small or too large, the segmentation boundaries are not satisfying. Because of the variety of mesh surfaces and the non-convexity of MS model, it is difficult to compute the parameter by a formula. However, according to the tests, α_0 can be set by the range $[1, 6]$.

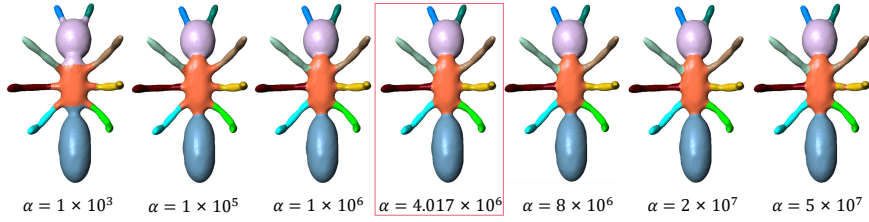


Figure 2: The segmentation results of different α by our GPSMS method with other parameters fixed.

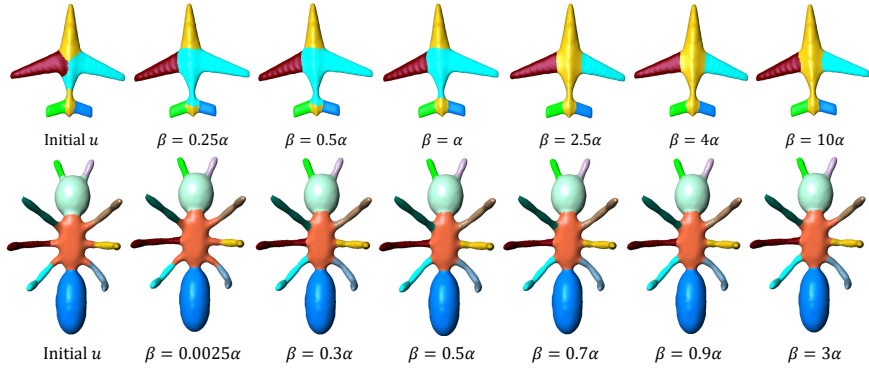


Figure 3: The segmentation results of different β by our GPSMS method with other parameters fixed.

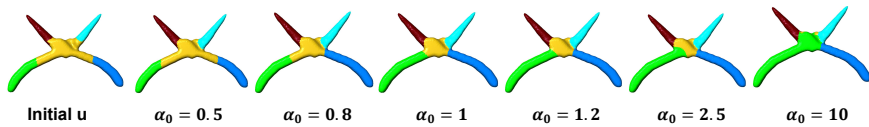


Figure 4: The segmentation results of different α_0 by our GPSMS method with other parameters fixed.

Remark 6.1. *The number of segment \mathbf{K} is affected by the geometric structure and semantic information of the mesh. It is difficult to find an empirical formula suitable for all mesh surfaces. In the paper, \mathbf{K} is set manually.*

6.2. Comparison to the piecewise constant MS method (PCMS) [11]

Since both our methods (including PSMS and GPSMS) and piecewise constant MS method (PCMS) [11] are based on the Mumford-Shah segmentation model, we would like to compare the three methods in more details, including the two-region segmentation results and the multi-region segmentation results.

6.2.1. Two-region segmentation

We first present the two-region segmentation results by the three methods and the corresponding \mathbf{g}, \mathbf{b} by our methods in Fig. 5 and 6.

As can be seen, for the Doublebell mesh in Fig. 5, the PCMS method produces results around the initialization no matter how to adjust the parameter, which is just the discontinuous position of the feature function (see the results in the first row of Fig. 5). By introducing the smooth function \mathbf{b} , the PSMS method can capture more structures of the mesh, and get results better than that of the PCMS method to a certain extent. However, the segmentation boundaries of the PSMS method are unitary and not optimal (see the results in the second row of Fig. 5, especially for the result in column (e)). By comparison, our GPSMS method exhibits the ability to acquire the different features of a mesh by using the RTGV regularization, which can identify the high order discontinuity of the feature function. Therefore, with appropriate parameter α_0 , the GPSMS method can get a variety of solutions consistent with the human cognition (see the results in the fifth row of Fig. 5).

In Fig. 6, we further test the three methods on the Pig mesh for two-region segmentation. Similarly, the PCMS method can capture the discontinuity of the feature function effectively, and thus are affected severely by the initialization. The PSMS method can improve the results to some extent (see the results in the second row of Fig. 6, especially for the result in column (c)). However, the role of smooth function \mathbf{b} is limited. By comparison, our GPSMS method not only get the discontinuity, but also characterize the high order discontinuous structures of the feature function effectively. The corresponding segmentation results are with better boundaries (see the results in the fifth row of Fig. 6, especially for the results in columns (b),(c),(d)).

6.2.2. Multi-region segmentation

We then present the multi-region segmentation results by the three methods.

Specifically, with the same initializations, we present the comparisons of the multi-region segmentation results produced by the three methods in Fig. 7. As observed, for the meshes in Fig. 7, the segmentation boundaries of the PCMS method are not perceptually good. The PCMS method is sensitive to geometric structures, and easily falls into local minima. It thus failed in getting the better boundaries (see the second row of Fig. 7). By introducing a new smooth function \mathbf{b} to the PCMS method, the PSMS method is able to alleviate the local minima case and find the better segmentation boundaries. Most segmentation results of the PSMS method is better than that of the PCMS method (see (a-f) of the third row of Fig. 7). In addition, as known, both the PCMS method and the PSMS method use the total variation regularization, which aims to get the shortest segmentation boundary. However, the shortest boundary is not always the optimal boundary (for example the mesh (g),(h),(i) in Fig. 7). Therefore, for meshes with extreme irregular structures (for examples the meshes (g-i) in Fig. 7), the PCMS method and the PSMS method fail in describe the structures. In contrast, the GPSMS method considers using a more general total variation regularization (the relaxed total generalized variation regularization), which involves second order differential operators and be able to capture more structures and overcome the staircase artifacts of TV regularization. It can relieve the influence of local minima and improve the segmentation boundaries. As can be seen from Fig. 7, the segmentation results of the GPSMS method are all satisfying (see the last row of Fig. 7). For the meshes in (a-f), the results of the PSMS method and the GPSMS method are similar, and are better than that of the PCMS method. For the meshes in (g-i), the segmentation results of the GPSMS method are better than that of the PCMS method and the PSMS method. In all, the GPSMS method displays the ability to depict the different levels of discontinuous information of the feature function of a mesh, and are more suitable for dealing with complex meshes.

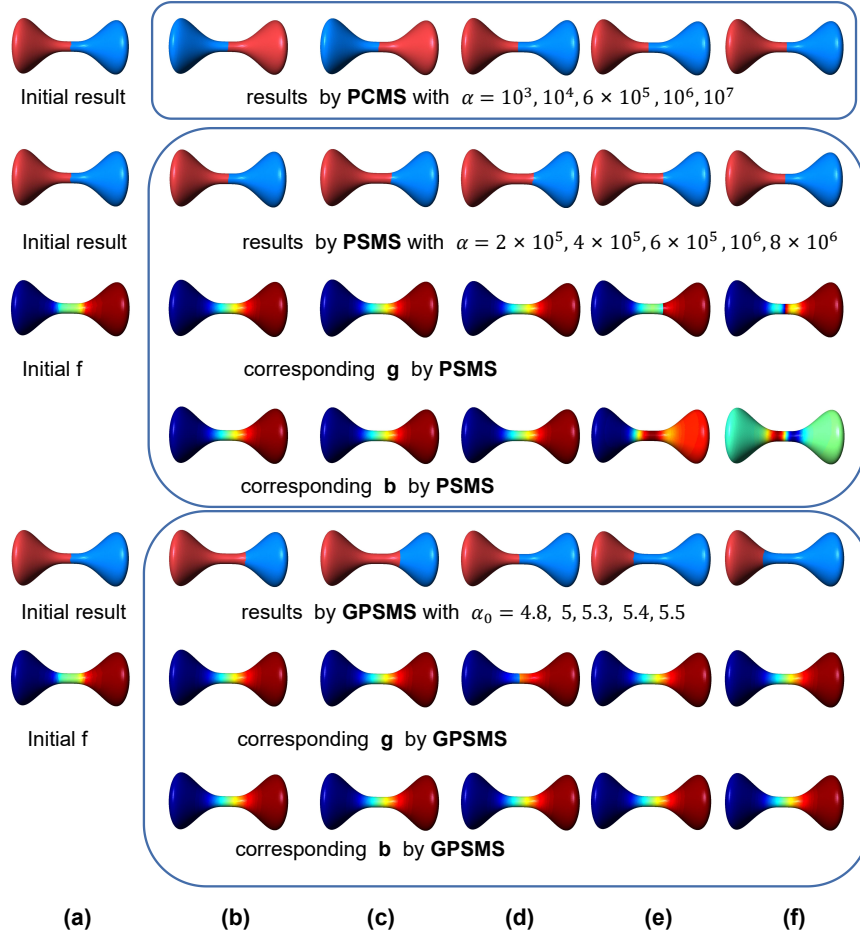


Figure 5: Comparisons of two-region segmentation results for Doublebell mesh by the PCMS method (the first row), the PSMS method (the second row), and the GPSMS method (the fifth row).

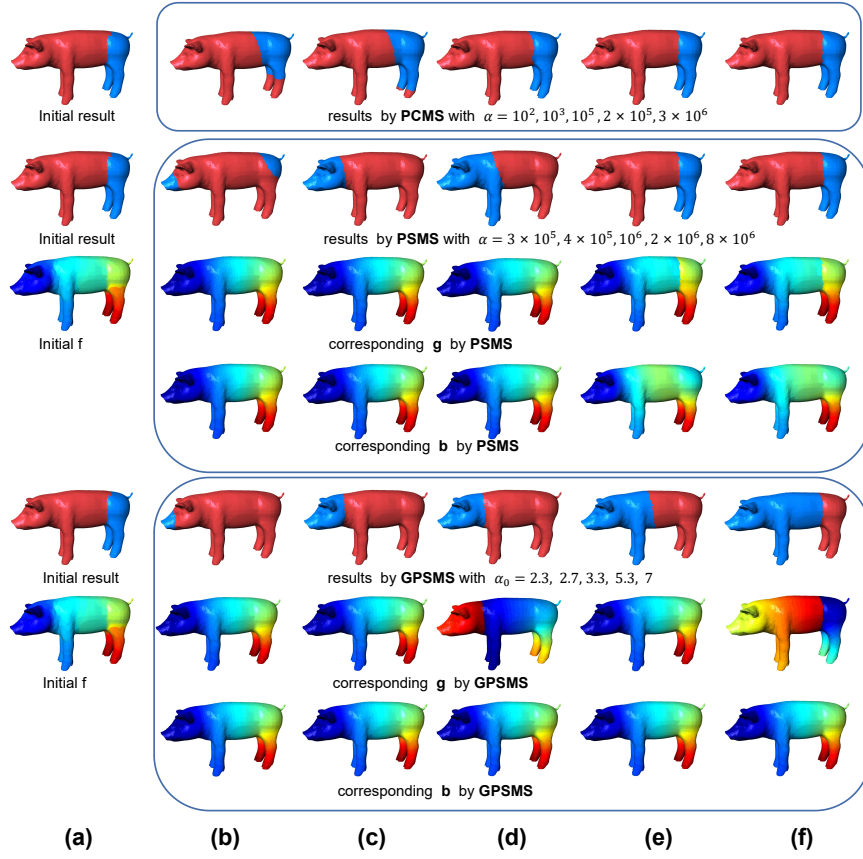


Figure 6: Comparisons of two-region segmentation results for Pig mesh by the PCMS method (the first row), the PSMS method (the second row), and the GPSMS method (the fifth row).

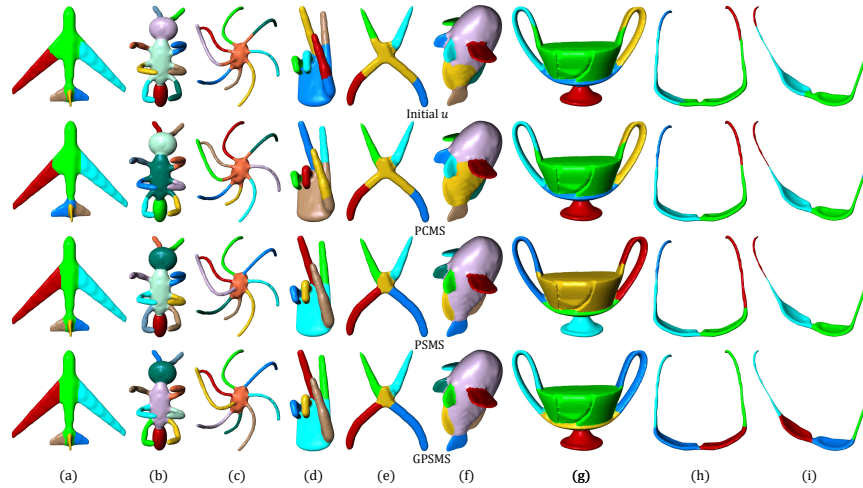


Figure 7: Comparisons of multi-region segmentation results. Initialization (The first row), PCMS (The second row), PSMS (The third row) and GPSMS (The last row).

6.3. Comparisons to other existing methods

In the section, we tested our GPSMS segmentation results on the Princeton Segmentation Benchmark [25], which contains 19 categories of 380 meshes for evaluating segmentation methods. With this benchmark, we also compare our approach both quantitatively and visually to Isoline Cut [26], WCSEg [27], PCMS [11], Spectral L_0 [29], SB19 [31] and PCN12 [32]. For evaluating the segmentation results, four evaluation metrics in [25] are used.

Figure 8 shows the results by our GPSMS method for representative meshes of the 19 categories in the Benchmark. As can be seen, our results are consistent with the semantics of human perception.

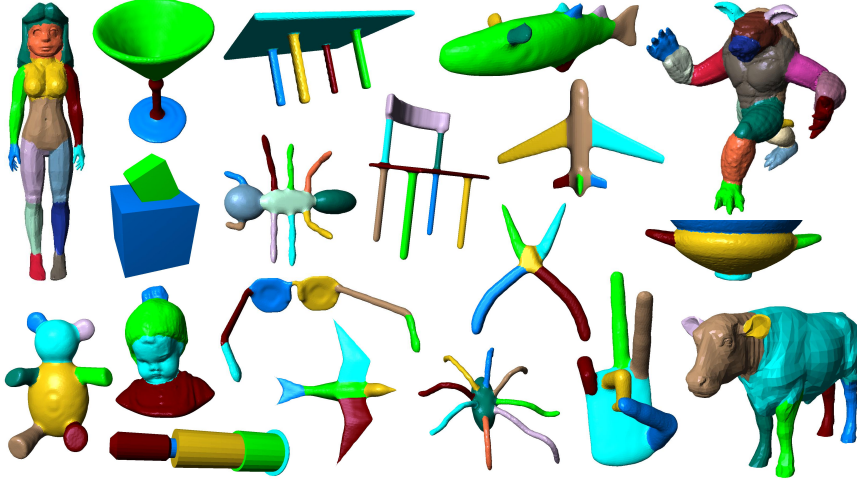


Figure 8: Representative segmentation results of 19 categories in Princeton Segmentation Benchmark by our GPSMS method.

Fig. 9 shows the quantitative comparisons between our GPSMS method and other methods according to the four error metrics in [25]. More details on the Rand Index (RI) metric are shown in Table 1, where the RI scores of all the compared methods for the 19 categories of meshes in Princeton Segmentation Benchmark are listed. We can see that the average RI errors of our results are lower than those of other methods. Fig. 10 further present the comparisons of segmentation results between our method and the Spectral L_0 method, respectively. As can be seen, the Spectral L_0 method either over segments the meshes or fails to capture the better boundaries (see the images marked by the red frames). By contrast, our method can produce results with better semantic parts and segmentation boundaries.

In addition to the benchmark data, we tested our algorithm on more meshes in Fig. 11, and our method can get satisfying results.

6.4. Computational cost

We now discuss the computational cost. The main computational cost is the iteratively solving the six sub problems in Algorithm 2. The main factors affecting the computational cost are mesh size, segmentation number and the parameter α . Meshes with large-size meshes or more segmentation parts consume longer computational time. We also find that if α is too small, the algorithm will be slow. Table 2 compares the CPU costs between our methods (PSMS and GPSMS) and the PCMS method for examples (a-d) in Fig. 7. As our methods introduce the new smooth variable \mathbf{b} and the RTGV regularization for the GPSMS method, the overall running time is longer than that of the PCMS method, especially for the GPSMS method. In addition, Fig. 12 presents the error curves with 100 iterations according to the absolute error $\|\mathbf{u}^l - \mathbf{u}^{l-1}\|_{\mathbf{U}_M}^2$ for results (a-d) in Fig. 7 by our PSMS method and GPSMS method, respectively. The error curves show that the errors within 100 iterations decreases fast, which also indicates that our algorithms are numerically robust.

6.5. Limitations

Our method has been demonstrated very effective in getting the better segmentation boundaries, but it still has some limitations. Firstly, we cannot give a formula to precisely compute the parameters and segmentation parts K .

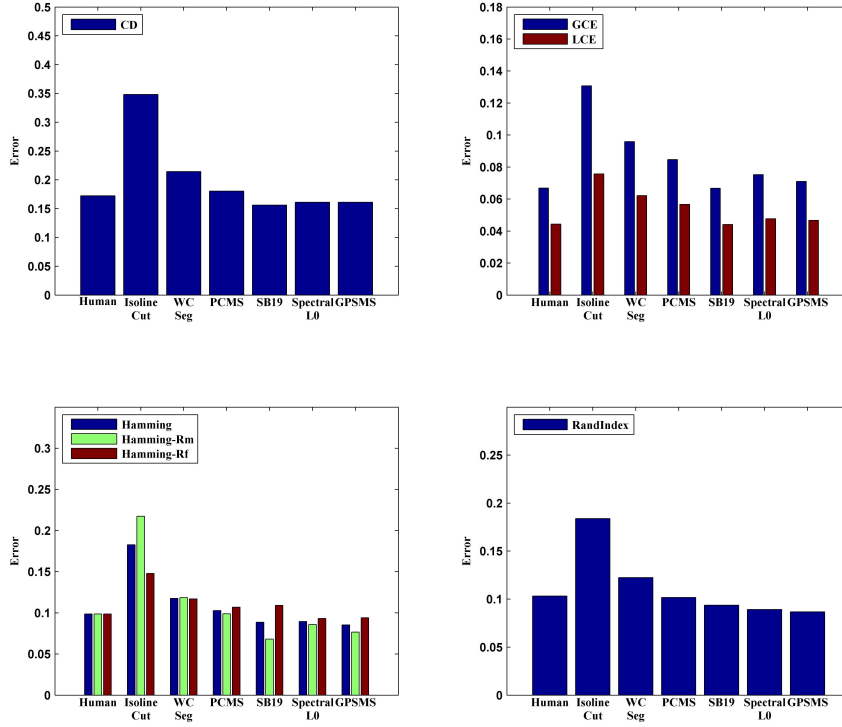


Figure 9: Evaluation of segmentation in terms of four evaluation metrics. The evaluations are performed according to the protocols and human segmentations in the Princeton Segmentation Benchmark of [25].

Table 1: Rand Index scores(the smaller the value, the better the segmentation results) across all 19 categories using our method and previous methods based on the Princeton Segmentation Benchmark of [25].

Categories	Human	IsolineCut	WC Seg	PCMS	SB19	SpectralL0	GPSMS
Human	13.8	12.5	12.8	13.0	12.0	12.84	12.83
Cup	13.6	26.1	17.1	10.1	10.0	11.05	9.37
Glasses	10.1	13.3	17.3	9.4	13.6	7.0	8.07
Airplane	9.2	19.7	8.9	10.5	7.9	8.4	8.39
Ant	3.0	4.5	2.1	2.2	1.8	1.86	1.87
Chair	8.9	9.0	10.3	6.8	5.4	5.68	6.19
Octopus	2.4	6.4	2.9	2.9	1.9	2.18	2.00
Table	9.3	13.5	9.1	6.6	5.6	6.0	6.04
Teddy	4.9	10.1	5.6	3.6	3.2	3.65	3.57
Hand	9.1	17.4	11.6	7.9	10.5	7.5	7.36
Plier	7.1	19.5	8.7	8.4	5.3	5.49	5.98
Fish	15.5	30.2	20.3	21.7	12.8	16.1	13.23
Bird	6.2	19.5	9.6	7.5	8.8	5.7	6.89
Armadillo	8.3	17.9	8.1	9.2	7.0	7.6	8.17
Bust	22.0	34.5	26.6	24.8	23.8	22.0	21.7
Mech	13.1	28.4	18.2	9.2	11.0	9.0	8.96
Bearing	10.4	28.6	11.9	10.7	9.1	8.6	8.06
Vase	14.4	18.0	16.1	12.6	14.7	10.8	11.18
FourLeg	14.9	20.3	15.2	15.9	13.8	17.76	14.83
Average	10.3	18.4	12.2	10.2	9.4	8.91	8.67

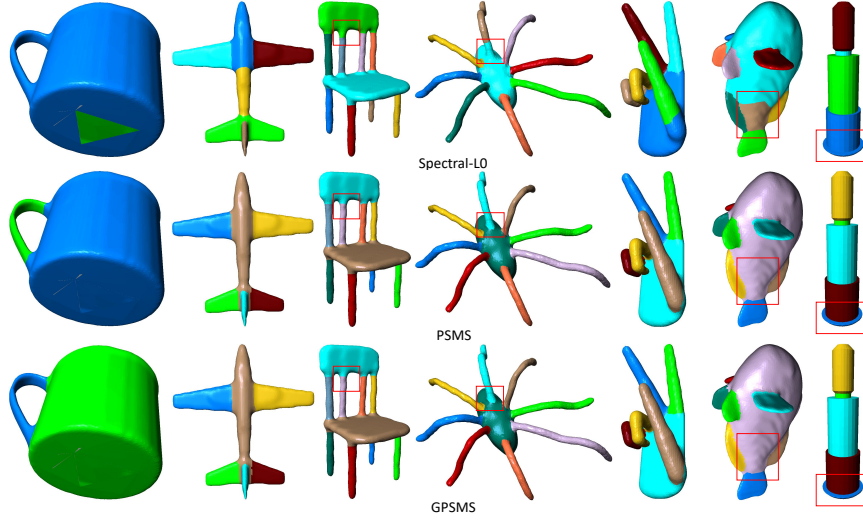


Figure 10: Comparison results between our segmentation method and the Spectral L_0 method [29].



Figure 11: The segmentation results of other models by our GPSMS method .

Table 2: Comparison of computational time (seconds) between our segmentation method and the PCMS method for surfaces in Fig. 7

Mesh	T	#Parts	PCMS	PSMS	GPSMS
Fig. 7 (a)	11162	6	0.24	0.83	1.9
Fig. 7 (b)	10624	11	1.4	2.3	7.1
Fig. 7 (c)	12646	9	0.21	1.1	2.4
Fig. 7 (d)	17044	6	0.4	1.5	4.6

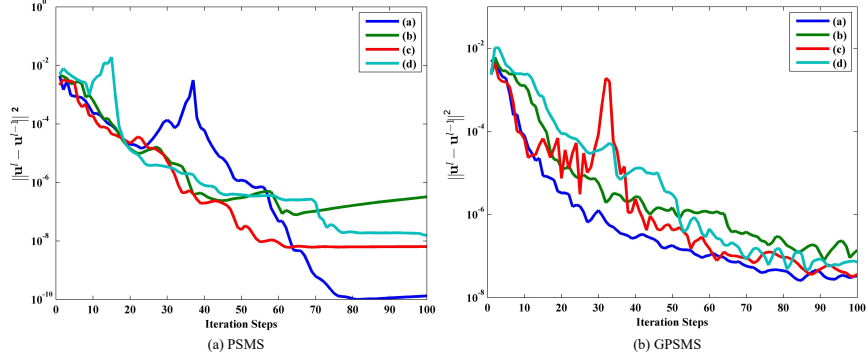


Figure 12: The absolute error $\|\mathbf{u}^{n+1} - \mathbf{u}^n\|_{U_M}^2$ with 100 iterations for examples (a-d) in Fig. 7 by our PSMS method and GPSMS method, respectively.

Secondly, for meshes with quite poor quality, our algorithm cannot give satisfying segmentation results; see Fig. 13 for an example. The mesh in Fig. 13(a) has very poor quality, in this case, we cannot get correct results (see Fig. 13(b-c)). Finally, as the Mumford-Shah model is non-convex, our method is thus affected by the clustering center μ due to the variant of the MS model.

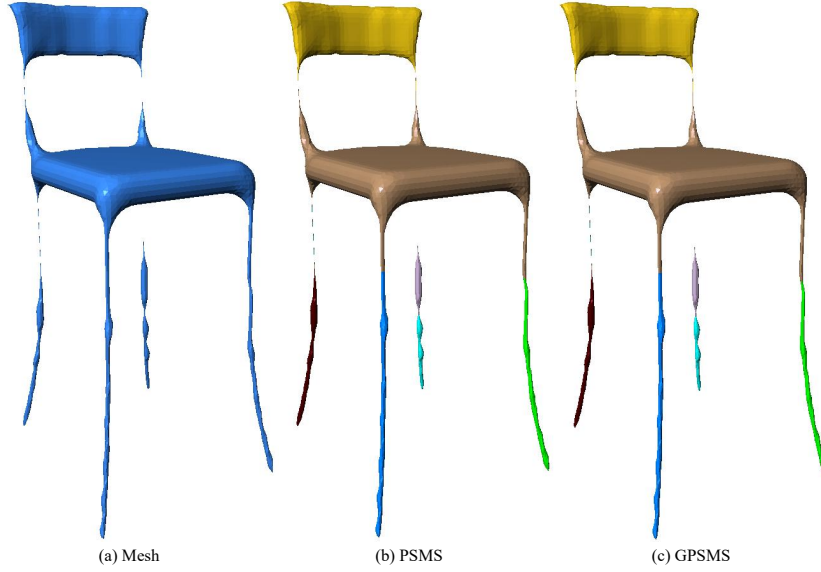


Figure 13: Failed results produced by our PSMS method and our GPSMS method.

7. Conclusions

The Mumford-Shah (MS) model is a vital tool for mesh segmentation, which pursues the shortest length of boundaries by the total variation regularization. The existing efforts try to solve the MS model through approximating the solutions with the piecewise constant functions. Different from most previous methods, in the article, we presented a novel piecewise smooth Mumford-Shah mesh segmentation technique using the total generalized variation regularization. The smooth model assumes to approximate the solutions by a sum of piecewise constant functions and a smooth function, and the TGV regularization involves the high order differential operator to characterize the high order discontinuous structures of the mesh. The proposed mesh segmentation method is effective in segmenting meshes

with irregular structures and getting the better boundaries. We solve our piecewise smooth MS method by the optimization iterative algorithm based on alternating minimization and ADMM, where the subproblems are solved by either the closed form solution or linear systems. Our algorithm is discussed from several aspects, including setting of parameters, computational costs, comparisons with piecewise constant MS model and evaluation on the Princeton Segmentation Benchmark with several state-of-art methods. Experimental results show that our piecewise smooth MS method can yield competitive results when compared to other approaches. Furthermore, the quantitative errors and computational costs further confirm the robustness and efficiency of the proposed method.

There are a few problems for further investigation. For instance, the preprocessing of the feature function of the mesh by the manifold learning techniques and the point cloud processing by the piecewise smooth MS model.

Acknowledgments

We would like to thank Pengfei Xu, Noa Fish, Weihua Tong for providing their segmentation data of [26], [27], [29], and the Princeton Segmentation Benchmark. The work is supported by the fund of Beijing Polytechnic, 2023X005-KXD.

References

- [1] D. Mumford, J. Shah, Optimal approximations by piecewise smooth functions and associated variational problems, *Commun. Pur. Appl. Math.* 42 (5) (1989) 577–685.
- [2] J. Lellmann, J. Kappes, J. Yuan, F. Becker, C. Schnoerr, Convex multi-class image labeling by simplex-constrained total variation, *Lecture Notes in Computer Science* 5567 (2009) 150–162.
- [3] J. Lellmann, C. Schnoerr, Continuous multiclass labeling approaches and algorithms, *SIAM J. Imaging Sci.* 4 (4) (2011) 1049–1096.
- [4] T. F. Chan, S. Esedoglu, M. Nikolova, Algorithms for finding global minimizers of image segmentation and denoising models, *SIAM journal on applied mathematics* 66 (5) (2006) 1632–1648.
- [5] A. Chambolle, Image segmentation by variational methods: Mumford and shah functional and the discrete approximations, *SIAM J. Appl. Math.* 55 (3) (1995) 827–863.
- [6] L. Vese, T. Chan, A multiphase level set framework for image segmentation using the mumford and shah model, *Int. J. Comput. Vis.* 50 (3) (2002) 271–293.
- [7] J. Lie, M. Lysaker, X.-C. Tai, A binary level set model and some applications for mumford-shah image segmentation, *IEEE Trans. Image Proc.* 15 (5) (2006) 1171–1181.
- [8] J. Lie, M. Lysaker, X.-C. Tai, A variant of the level set method and applications to image segmentation, *Mathematics of computation* 75 (255) (2006) 1155–1174.
- [9] E. Brown, T. Chan, X. Bresson, Completely convex formulation of the chan-vese image segmentation model, *Int. J. Comput. Vis.* 98 (1) (2012) 103–121.
- [10] J. Zhang, J. Zheng, C. Wu, J. Cai, Variational mesh decomposition, *ACM Trans. Graph.* 31 (3) (2012) 21.
- [11] H. Zhang, C. Wu, J. Deng, Z. Liu, Y. Yang, A new two-stage mesh surface segmentation method, *The Visual Computer* 34 (2018) 1597–1615.
- [12] T. Le, L. Vese, Additive and multiplicative piecewise-smooth segmentation models in a functional minimization approach, *Interpolation Theory and Applications* 445 (3) (2007) 207–224.
- [13] Y. Gu, W. Xiong, L.-L. Wang, J. Cheng, Generalizing mumford-shah model for multiphase piecewise smooth image segmentation, *IEEE Transactions on Image Processing* 26 (2) (2016) 942–952.
- [14] F. Li, M. K. Ng, C. Li, Variational fuzzy mumford-shah model for image segmentation, *SIAM Journal on Applied Mathematics* 70 (7) (2010) 2750–2770.
- [15] Y. Gu, L.-L. Wang, W. Xiong, J. Cheng, W. Huang, J. Zhou, Efficient and robust image segmentation with a new piecewise-smooth decomposition model, in: *2013 IEEE International Conference on Image Processing, IEEE, 2013*, pp. 2718–2722.
- [16] M. Jung, Piecewise-smooth image segmentation models with 11 data-fidelity terms, *Journal of Scientific Computing* 70 (3) (2017) 1229–1261.
- [17] Y. Li, C. Wu, Y. Duan, The tvp regularized mumford-shah model for image labeling and segmentation, *IEEE Transactions on Image Processing* 29 (2020) 7061–7075.
- [18] K. Bredies, K. Kunisch, T. Pock, Total generalized variation, *SIAM Journal on Imaging Sciences* 3 (3) (2010) 492–526.
- [19] H. Zhang, Z. He, X. Wang, A novel mesh denoising method based on relaxed second-order total generalized variation, *SIAM Journal on Imaging Sciences* 15 (1) (2022) 1–22.
- [20] S. Wang, H. Zhang, Total generalized variation regularized piecewise smooth mumford-shah point cloud surface segmentation, *Academic Journal of Computing and Information Science* 7 (5).
- [21] L. Ambrosio, V. M. Tortorelli, Approximation of functional depending on jumps by elliptic functional via t-convergence, *Communications on Pure and Applied Mathematics* 43 (8) (1990) 999–1036.
- [22] A. Shamir, A survey on mesh segmentation techniques, *Comput. Graph. Forum* 27 (6) (2008) 1539–1556.
- [23] A. Agathos, I. Pratikakis, S. Perantonis, P. Azariadis, 3d mesh segmentation methodologies for cad applications, *Computer-Aided Design and Applications* 4 (6) (2007) 827–841.
- [24] R. S. Rodrigues, J. F. Morgado, A. J. Gomes, Part-based mesh segmentation: a survey, in: *Computer Graphics Forum, Vol. 37, Wiley Online Library, 2018*, pp. 235–274.

- [25] X. Chen, A. Golovinskiy, T. Funkhouser, A benchmark for 3d mesh segmentation, in: Siggraph, 2009, pp. 1–12.
- [26] O. Au, Y. Zheng, M. Chen, P. Xu, C. Tai, Mesh segmentation with concavity aware fields, IEEE Trans. Vis. Comput. Graph. 18 (7) (2012) 1125–1134.
- [27] O. Kaick, N. Fish, Y. Kleiman, S. Asafi, D. Cohen-Or, Shape segmentation by approximate convexity analysis, ACM Trans. Graph. 34 (1) (2014) 1–11.
- [28] N. Bonneel, D. Coeurjolly, P. Gueth, J.-O. Lachaud, Mumford-shah mesh processing using the ambrosio-tortorelli functional, Computer Graphics Forum 37 (7) (2018) 75–85.
- [29] W. Tong, X. Yang, M. Pan, F. Chen, Spectral mesh segmentation via l_0 gradient minimization, IEEE transactions on visualization and computer graphics 26 (4) (2020) 1807–1820.
- [30] H. Zhang, C. Wang, Total variation diffusion and its application in shape decomposition, Computers and Graphics 90 (2020) 95–107.
- [31] E. Kalogerakis, A. Hertzmann, K. Singh, Learning 3d mesh segmentation and labeling, ACM Trans. Graph. 29 (3) (2010) 1–12.
- [32] E. Kalogerakis, M. Averkiou, S. Maji, S. Chaudhuri, 3d shape segmentation with projective convolutional networks, in: CVPR, 2017, pp. 3779–3788.
- [33] T. Le, G. Bui, Y. Duan, A multi-view recurrent neural network for 3d mesh segmentation, Computers and Graphics 66 (2017) 103–112.
- [34] A. Lahav, A. Tal, Meshwalker: Deep mesh understanding by random walks, ACM Transactions on Graphics (TOG) 39 (6) (2020) 1–13.
- [35] Q. Dong, Z. Wang, M. Li, J. Gao, S. Chen, Z. Shu, S. Xin, C. Tu, W. Wang, Laplacian2mesh: Laplacian-based mesh understanding, IEEE Transactions on Visualization and Computer Graphics.
- [36] H. Zhang, C. Wu, J. Zhang, J. Deng, Variational mesh denoising using total variation and piecewise constant function space, IEEE Trans. Vis. Comput. Graph. 21 (7) (2015) 873–886.
- [37] J. Shi, J. Malik, Normalized cuts and image segmentation, IEEE Trans. Pattern Anal. Mach. Intell. 22 (8) (2000) 888–905.
- [38] V. L. U, A tutorial on spectral clustering, Statistics and computing 17 (2007) 395–416.
- [39] R. Liu, H. Zhang, Segmentation of 3d meshes through spectral clustering, in: Proceedings of the Pacific Conference on Computer Graphics and Applications, 2004, pp. 298–305.
- [40] C. Wu, X. Tai, Augmented lagrangian method, dual methods, and split bregman iteration for rof, vectorial tv, and high order models, SIAM J. Imaging Sci. 3 (3) (2010) 300–339.
- [41] J. Yang, Y. Zhang, W. Yin, A fast alternating direction method for tvl1-l2 signal reconstruction from partial fourier data, IEEE Journal of Selected Topics in Signal Processing 4 (2) (2010) 288–297.
- [42] M. NG, P. Weiss, X. Yuan, Solving constrained total-variation image restoration and reconstruction problems via alternating direction methods, SIAM J. Sci. Comput. 32 (5) (2010) 2710–2736.
- [43] S. Boyd, N. Parikh, E. Chu, B. Peleato, J. Eckstein, Distributed optimization and statistical learning via the alternating direction method of multipliers, Foundations and Trends in Machine Learning 3 (1) (2011) 1–122.
- [44] C. Michelot, A finite algorithm for finding the projection of a point onto the canonical simplex of r^n , J. Optim. Theory Appl. 50 (1) (1986) 195–200.

Proof of Theorem 1

Proof 1. As the energy E is positive, proper, and bounded from below by zero, let $(\mathbf{u}^n, \mathbf{b}^n, \mu^n)$ be a minimizing sequence of (13) that satisfies

$$E(\mathbf{u}^n, \mathbf{b}^n, \mu^n) \rightarrow \inf E(\mathbf{u}, \mathbf{b}, \mu), \quad n \rightarrow \infty.$$

Then, there exists a $M > 0$ such that $E(\mathbf{u}^n, \mathbf{b}^n, \mu^n) \leq M$. This implies that each term in $E(\mathbf{u}^n, \mathbf{b}^n, \mu^n)$ is bounded. That is

$$\text{GTV}^p(\mathbf{u}) \leq M, \quad \|\Delta \mathbf{b}\|^2 \leq M, \quad \|\mathbf{b}\|^2 \leq M, \quad \langle \mathbf{u}, s(\mathbf{f}, \mathbf{b}, \mu) \rangle_{U_M} \leq M.$$

Moreover, since $\mathbf{u}_k^n \in [0, 1]$, we conclude that $\{\mathbf{u}^n\}$ is bounded in $\text{BV}(\Omega)$. By the compact embedding theorem, there exists a subsequence $\{\mathbf{u}^{n_i}\}$ convergent to \mathbf{u}^* in $L^1(\Omega)$.

Meanwhile, as $\{\mu_k^n\}$ is bounded, we can get a subsequence $\{\mu_k^{n_i}\}$ converge to a constant $\{\mu_k^*\}$.

In addition, we note that

$$\int_{\Omega} |\mathbf{b}^n|^2 dx < M, \quad \int_{\Omega} |\Delta \mathbf{b}^n|^2 dx < M.$$

This show that $\{\mathbf{b}^n\}$ is also bounded. Therefore, it exists a subsequence $\{\mathbf{b}^{n_i}\}$ that converges to \mathbf{b}^* in $L^2(\Omega)$. Then, by the lower semi-continuity, we have

$$\text{GTV}^p(\mathbf{u}^*) \leq \liminf_{n \rightarrow \infty} \text{GTV}^p(\mathbf{u}^n),$$

$$\|\Delta \mathbf{b}^*\|^2 \leq \liminf_{n \rightarrow \infty} \|\Delta \mathbf{b}^n\|^2,$$

$$\|\mathbf{b}^*\|^2 \leq \liminf_{n \rightarrow \infty} \|\mathbf{b}^n\|^2.$$

Moreover, by the Fatou's lemma, we get

$$\langle \mathbf{u}^*, s(\mathbf{f}, \mathbf{b}^*, \mu^*) \rangle_{U_M} \leq \liminf_{n \rightarrow \infty} \langle \mathbf{u}^n, s(\mathbf{f}, \mathbf{b}^n, \mu^n) \rangle_{U_M}.$$

We then have

$$E(\mathbf{u}^*, \mathbf{b}^*, \mu^*) \leq \liminf_{n \rightarrow \infty} E(\mathbf{u}^n, \mathbf{b}^n, \mu^n) = \inf E(\mathbf{u}, \mathbf{b}, \mu),$$

which implies that $(\mathbf{u}^*, \mathbf{b}^*, \mu^*)$ is a minimizer of problem (13).

Proof of Theorem 2

Proof 2. By the Lagrange multiplier formulas, we have

$$\begin{aligned} \lim_{l \rightarrow \infty} r_{\mathbf{p}}^{-1}(\lambda_{\mathbf{p}}^l - \lambda_{\mathbf{p}}^{l-1}) &= \lim_{k \rightarrow \infty} \mathbf{p}^l - (\nabla \mathbf{u}^l - \mathbf{v}^l) = \mathbf{p}^* - (\nabla \mathbf{u}^* - \mathbf{v}^*) = 0, \\ \lim_{l \rightarrow \infty} r_{\mathbf{q}}^{-1}(\lambda_{\mathbf{q}}^l - \lambda_{\mathbf{q}}^{l-1}) &= \lim_{k \rightarrow \infty} \mathbf{q}^l - \text{div}(w\mathbf{v}^l) = \mathbf{q}^* - \text{div}(w\mathbf{v}^*) = 0, \\ \lim_{l \rightarrow \infty} r_{\mathbf{z}}^{-1}(\lambda_{\mathbf{z}}^l - \lambda_{\mathbf{z}}^{l-1}) &= \lim_{k \rightarrow \infty} \mathbf{z}^l - \mathbf{u}^l = \mathbf{z}^* - \mathbf{u}^* = 0. \end{aligned} \quad (.1)$$

The optimization conditions of $\mathbf{u}, \mathbf{v}, \mathbf{b}, \mu$ sub-problems are

$$\begin{aligned} -\lambda_{\mathbf{z}}^{l-1} + r_{\mathbf{z}}(\mathbf{u}^l - \mathbf{z}^{l-1}) + \text{div}(\lambda_{\mathbf{p}}^{l-1}) - r_{\mathbf{p}}\text{div}(\nabla \mathbf{u}^l - \mathbf{v}^{l-1} - \mathbf{p}^{l-1}) &= 0, \\ \lambda_{\mathbf{p}}^{l-1} + r_{\mathbf{p}}(\mathbf{v}^l - (\nabla \mathbf{u}^l - \mathbf{p}^{l-1})) + \nabla(\lambda_{\mathbf{q}}^{l-1}) - r_{\mathbf{q}}\nabla(\text{div}(\mathbf{v}^l) - \mathbf{q}^{l-1}) &= 0, \\ (\beta\Delta^2 + \eta\mathcal{I} + \alpha\mathcal{I})\mathbf{b}^l + \alpha < -(\mathbf{f} - \mu^{l-1}), \mathbf{z}^{l-1} > &= 0, \\ \alpha < \mu^l - (\mathbf{f} - \mathbf{b}^l), \mathbf{u}^l > &= 0. \end{aligned} \quad (.2)$$

We rearrange above formulas and get

$$\begin{aligned} -\lambda_{\mathbf{z}}^{l-1} + r_{\mathbf{z}}(\mathbf{u}^l - \mathbf{u}^{l-1} + \mathbf{u}^{l-1} - \mathbf{z}^{l-1}) + \text{div}(\lambda_{\mathbf{p}}^{l-1}) \\ - r_{\mathbf{p}}\text{div}(\nabla \mathbf{u}^l - \mathbf{v}^l - \mathbf{p}^l + \mathbf{v}^l - \mathbf{v}^{l-1} + \mathbf{p}^l - \mathbf{p}^{l-1}) &= 0, \\ \lambda_{\mathbf{p}}^{l-1} + r_{\mathbf{p}}(\mathbf{v}^l - (\nabla \mathbf{u}^l - \mathbf{p}^l + \mathbf{p}^l - \mathbf{p}^{l-1})) + \nabla(\lambda_{\mathbf{q}}^{l-1}) \\ - r_{\mathbf{q}}\nabla(\text{div}(\mathbf{v}^l) - \mathbf{q}^l + \mathbf{q}^l - \mathbf{q}^{l-1}) &= 0, \\ (\beta\Delta^2 + \eta\mathcal{I} + \alpha\mathcal{I})\mathbf{b}^l + \alpha < -(\mathbf{f} - \mu^l + \mu^l - \mu^{l-1}), \mathbf{z}^l - \mathbf{z}^l + \mathbf{z}^{l-1} > &= 0, \\ \alpha < \mu^l - (\mathbf{f} - \mathbf{b}^l), \mathbf{u}^l > &= 0. \end{aligned} \quad (.3)$$

By taking the limit $l \rightarrow \infty$, we get

$$\begin{aligned} -\lambda_{\mathbf{z}}^* + \text{div}(\lambda_{\mathbf{p}}^*) &= 0, \lambda_{\mathbf{p}}^* + w\nabla(\lambda_{\mathbf{q}}^*) = 0, \\ (\beta\Delta^2 + \eta\mathcal{I} + \alpha\mathcal{I})\mathbf{b}^* + \alpha < -(\mathbf{f} - \mu^*), \mathbf{z}^* > &= 0, \\ \alpha < \mu^* - (\mathbf{f} - \mathbf{b}^*), \mathbf{u}^* > &= 0. \end{aligned} \quad (.4)$$

Next, we consider the optimality conditions of $\mathbf{p}, \mathbf{q}, \mathbf{z}$ sub-problems

$$\begin{aligned} \partial(\|\mathbf{p}^l\|_1) + \lambda_{\mathbf{p}}^{l-1} + r_{\mathbf{p}}(\mathbf{p}^l - (\nabla \mathbf{u}^l - \mathbf{v}^l)) &\ni 0, \\ \alpha_0\partial(\|\mathbf{q}^l\|_1) + \lambda_{\mathbf{q}}^{l-1} + r_{\mathbf{q}}(\mathbf{q}^l - \text{div}(\mathbf{v}^l)) &\ni 0, \\ \alpha s(\mathbf{f}, \mathbf{b}^l, \mu^l) + \partial\mathcal{X}(\mathbf{z}^l) + \lambda_{\mathbf{z}}^l + r_{\mathbf{z}}(\mathbf{z}^l - \mathbf{u}^l) &\ni 0. \end{aligned} \quad (.5)$$

Then, in the limits $k \rightarrow \infty$, we obtain

$$\begin{aligned} \partial(\|\mathbf{p}^*\|_1) + \lambda_{\mathbf{p}}^* &\ni 0, \\ \alpha_0\partial(\|\mathbf{q}^*\|_1) + \lambda_{\mathbf{q}}^* &\ni 0, \\ \alpha s(\mathbf{f}, \mathbf{b}^*, \mu^*) + \partial\mathcal{X}(\mathbf{z}^*) + \lambda_{\mathbf{z}}^* &\ni 0. \end{aligned} \quad (.6)$$